Nano Research

Open Access

Research Article

A sodium-templated structure search reveals a topological semimetal silicon anode for sodium-ion batteries

Huanhuan Xie[1,2], Yingnan Song[1], Kehan Zhang[1], Jiakang Shi[1], and Young Hee Lee[2,3,4]

[1] *Key Laboratory of Magnetic Molecules and Magnetic Information Materials of the Ministry of Education & School of Materials Science and Engineering, Shanxi Normal University, Taiyuan 030031, China*
[2] *Center for Integrated Nanostructure Physics (CINAP), Sungkyunkwan University, Suwon 16419, Republic of Korea*
[3] *Center for Low-Dimensional Quantum Materials, Hubei University of Technology, Wuhan 430062, China*
[4] *School of Materials Science and Engineering, Peking University, Beijing 100871, China*

Cite this article: *Nano Research*, **2026**, *19*, 94908585. https://doi.org/10.26599/NR.2026.94908585

ABSTRACT: We report a porous Na–Si framework ($NaSi_4$) identified via a Na-templated crystal structure search, which integrates nontrivial topological electronic states with high-performance sodium-ion storage. $NaSi_4$ crystallizes in an orthorhombic architecture consisting of interpenetrating sp^3-bonded silicon frameworks that form one-dimensional Na-filled channels. Upon Na removal, the resulting silicon host (Si_{16}) preserves the open-channel topology and structural integrity. Electronic structure calculations reveal symmetry-protected band crossings near the Fermi level, establishing Si_{16} as a topological nodal-line semimetal with intrinsically robust electronic conductivity. Benefiting from the built-in conductivity and accessible diffusion channels, the Si_{16} framework delivers a high reversible Na-storage capacity of ~ 239 mAh·g^{-1} at an average insertion voltage of ~ 0.52 V (vs. Na/Na$^+$). First-principles calculations further indicate strong Na binding, fast one-dimensional Na$^+$ migration, and excellent structural stability. This work demonstrates a viable Na-templated design strategy for multifunctional silicon anodes and highlights the potential of coupling topological electronic states with energy-storage materials.

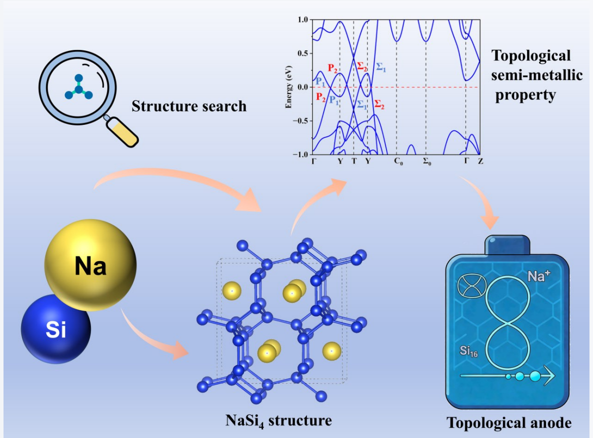

KEYWORDS: sodium-ion batteries, porous silicon anode, Na-templated structure search, nodal-line semimetal

1 Introduction

The rapidly growing demand for large-scale and low-cost energy storage systems has stimulated intensive research beyond conventional lithium-ion batteries (LIBs) [1–4]. Among various alternatives, sodium-ion batteries (SIBs) have emerged as particularly attractive candidates owing to the natural abundance, low cost, and favorable sustainability of sodium resources [5–7]. However, the development of high-performance anode materials for SIBs remains a critical bottleneck, primarily due to the larger ionic radius (~ 1.02 Å) and heavier mass of Na$^+$ compared with Li$^+$, which lead to sluggish diffusion kinetics, limited reversible capacity, and severe structural instability in many host materials [8–10]. Notably, graphite can only accommodate Na in a very limited staged compound (NaC_{64}), corresponding to a negligible capacity of ~ 35 mAh·g^{-1}, rendering graphite unsuitable for practical SIB anodes and motivating the search for new electrode materials beyond graphitic carbon [11–14].

Silicon-based anodes, well known for their ultrahigh theoretical capacity in LIBs, have recently attracted increasing attention in the context of SIBs [15]. Nevertheless, crystalline and amorphous Si frameworks generally suffer from poor Na$^+$ accommodation, large volume expansion, and low electronic conductivity, rendering direct application highly challenging [15]. For example, bulk diamond-structure Si can alloy with Na, but typically at the cost of massive volumetric expansion and degradation of electrical connectivity, as commonly observed in amorphous Na–Si alloys. Meanwhile, carbon-based anodes, such as amorphous hard carbon, can deliver 200–300 mAh·g^{-1} capacity for Na-storage, yet their

Received: January 21, 2026; **Revised:** February 6, 2026
Accepted: February 15, 2026

Address correspondence to Huanhuan Xie, 20210090@sxnu.edu.cn; Young Hee Lee, leeyoung@skku.edu

disordered porosity and structural defects often impede Na^+ transport and electronic conductivity, further underscoring that rational structural design strategies simultaneously addressing Na^+ storage space, diffusion pathways, and electronic transport are urgently required [16–18]. To overcome these intrinsic limitations, rational structural design strategies that simultaneously address Na^+ storage space, diffusion pathways, and electronic transport are urgently required [19, 20].

Porous framework materials offer a promising solution in this regard [21, 22]. In particular, three-dimensional (3D) open frameworks with ordered channels can effectively alleviate volume strain while enabling fast ion transport. Meanwhile, metallic or semimetallic electronic structures are highly desirable to guarantee sufficient electronic conductivity without relying on conductive additives [23, 24]. From a fundamental perspective, topological semimetals (TSM)—characterized by symmetry-protected band crossings and high carrier mobility—represent an emerging class of quantum materials that naturally satisfy the electronic requirements of battery electrodes [25–27]. Three-dimensional TSM allotropes integrate intrinsic metallicity with ordered pores for Na^+ storage, as exemplified by porous tetragonal C_{24} (tC_{24}), which exhibits moderate capacity, ultralow Na^+ diffusion barriers, and negligible volume change [28]. Despite such appealing transport and electrochemical characteristics, topological materials have rarely been explored in electrochemical energy storage, and the rational design of electrode materials that intrinsically combine porosity, ionic functionality, and nontrivial band topology remains largely unexplored.

Here, we demonstrate that these challenges can be addressed through a targeted structure-search strategy based on chemical pre-sodiation. Instead of performing conventional crystal structure searches on sodium-free silicon frameworks, we explicitly introduce Na atoms as structural and chemical templates during the global structure search. This strategy is motivated by the physical insight that pre-inserted Na can actively regulate Si–Si bonding motifs, stabilize open frameworks during structure evolution, and predefine Na^+ diffusion channels. By subsequently removing or partially extracting Na, one can obtain metastable porous silicon-based frameworks that are intrinsically compatible with Na^+ insertion and extraction processes. The feasibility of alkali-metal templating for open-framework silicon has been demonstrated experimentally by the synthesis of the porous silicon allotrope Si_{24} (open-cage Si_{24}), obtained by quenching Na_4Si_{24} formed under high pressure, followed by Na removal [29].

Using this pre-sodiated structure-search approach implemented within the crystal structure analysis by particle swarm optimization (CALYPSO) framework, we identify a previously unreported $NaSi_4$ phase that exhibits a three-dimensional open Si network with ordered channels suitable for Na^+ storage and migration. Remarkably, beyond its favorable structural features for SIB anodes, we show that the sodium-free framework (Si_{16}) is a topological nodal-line semimetal (TNSM) featuring two distinct symmetry-protected band-crossing loops near the Fermi level (E_F), thereby providing intrinsic electronic conductivity. The coexistence of intrinsic porosity and topological semimetallicity endows this material with both fast Na^+ diffusion kinetics and high electronic conductivity—two key requirements for high-rate and long-life SIB anodes. Comprehensive first-principles calculations reveal that $NaSi_4$ is dynamically, thermally, and mechanically stable, and exhibits low Na^+ migration barriers along the intrinsic channels, moderate sodiation voltage, and limited volume variation during Na insertion/extraction. More importantly, our work establishes chemical pre-sodiation-assisted structure search as a general and physically transparent route for discovering functional electrode materials that would be difficult to access via conventional structure prediction schemes.

By bridging sodium-ion battery chemistry with topological quantum materials, this study not only proposes $NaSi_4$ as a promising SIB anode candidate but also highlights a new design paradigm for multifunctional energy materials. In this paradigm, chemical pre-sodiation enables the simultaneous optimization of ordered porous channels for Na^+ storage and minimized mechanical degradation via low-strain sodiation/desodiation.

2 Computational methods

2.1 Crystal structure prediction

To explore possible Na–Si frameworks, a comprehensive crystal structure search was performed for a series of compositions $NaSi_x$ (x = 1–6) using the CALYPSO code [30]. This method employs a particle swarm optimization (PSO) algorithm inspired by biological evolution to efficiently locate low-enthalpy configurations [31]. For each stoichiometry, simulation cells containing 1–8 formula units were considered to ensure sufficient structural diversity. The structural evolution proceeded over 50 generations, each comprising 30 candidate structures. To balance global exploration and local optimization, 60% of the lowest-enthalpy structures from each generation were selected for heredity, while the remaining 40% were generated randomly to maintain configurational diversity. Through this global search across the Na–Si compositional space, the $NaSi_4$ composition was identified as exhibiting the lowest enthalpy among the porous framework candidates and the most favorable open-framework geometry within the explored $NaSi_x$ (x = 1–6) range, and was therefore selected for detailed analysis. This hybrid evolutionary strategy ensures robust convergence toward low-enthalpy configurations on the energy landscape and enables reliable identification of energetically competitive Na–Si framework structures, including metastable candidates.

2.2 First-principles calculations

Density functional theory (DFT) calculations were performed using the Vienna *ab initio* simulation package (VASP) [32, 33]. The projected augmented wave (PAW) method was used to treat core–valence interactions, and a plane-wave basis with a 600 eV kinetic energy cutoff was employed [34]. The Perdew–Burke–Ernzerhof (PBE) generalized gradient approximation was used for the exchange-correlation functional [35]. Brillouin zone (BZ) sampling was done with Monkhorst–Pack k-meshes dense enough to achieve a resolution of $2\pi \times 0.02$ Å^{-1} in reciprocal space [36]. Structural relaxations were run until forces on all atoms were below 0.01 eV·Å^{-1} and energy changes below 10^{-4} eV. More stringent criteria (10^{-6} eV energy, 10^{-4} eV·Å^{-1} forces) were applied for high-precision calculations, such as phonon and *ab initio* molecular dynamics (AIMD) simulations. Phonon dispersion relations were computed using density functional perturbation theory (DFPT) as implemented in the DS-PAW module of Device Studio [37]. Spin-orbit coupling (SOC) effects were investigated and found to have negligible influence on both the band structure and the topological nodal line properties of the system. The negligible SOC effect mainly originates from the light atomic masses of Si and Na, which result in weak relativistic interactions. After achieving self-consistency, maximally localized Wannier functions [38] were constructed using Si s and p orbitals. The slab band structure, bulk band structure, and its topological properties were subsequently calculated using the WannierTools package [39]. Sodium-ion diffusion barriers were evaluated using the climbing image nudged elastic band (CI-NEB) method [40].

2.3 Cluster expansion method

To model the configurational energetics of partially sodiated Na_xSi_4 ($0 \le x \le 1$) structures, we employed the cluster expansion (CE) approach as implemented in the Alloy Theoretic Automated Toolkit (ATAT) [41, 42]. In this framework, each potential Na site is represented by a binary occupation variable (σ_i), where $\sigma_i = +1$ if occupied by Na and $\sigma_i = -1$ if vacant. The total energy of a configuration ($E(\sigma)$) is expressed as a generalized Ising-like expansion over lattice clusters

$$E(\sigma) = J_0 + \sum_i J_i \sigma_i + \sum_{i<j} J_{ij} \sigma_i \sigma_j + \sum_{i<j<k} J_{ijk} \sigma_i \sigma_j \sigma_k + \cdots = J_0 + \sum_\alpha J_\alpha \phi_\alpha \qquad (1)$$

where J_0 is the reference energy; J_i, J_{ij}, and J_{ijk} are the effective cluster interactions for single-site, pair, and triplet clusters, respectively. The subscript α denotes a general cluster, and ϕ_α is the corresponding cluster function, defined as the product of occupation variables over the sites belonging to cluster α. J_α are the effective cluster interactions (ECIs), and the summation runs over all distinct clusters (points, pairs, triplets, etc.).

A diverse set of Na_xSi_4 structures spanning various Na concentrations and configurations was generated, and their total energies were calculated via DFT. The accuracy of the resulting CE model was validated by a cross-validation (CV) score below 15 meV·f.u.$^{-1}$ (f.u.: formula unit), ensuring reliable prediction of intermediate configurations.

3 Results and discussion

3.1 Crystal structure of $NaSi_4$ and porous silicon framework

Figure 1(a) depicts the optimized crystal structure of $NaSi_4$ obtained from our global search. The compound crystallizes in an orthorhombic lattice with the space group *Cmcm* (No. 63). Its unit cell contains 16 Si and 4 Na atoms, corresponding to the chemical formula $NaSi_4$. The structure can be described as a porous silicon framework with Na atoms residing in one-dimensional (1D) channels. Each silicon atom is fourfold coordinated and exhibits sp^3 hybridized, forming a covalent network that is interwoven to create tunnel-like pores. The Na atoms occupy the center of these tunnels, as indicated by the yellow spheres, while the silicon host framework, shown as blue spheres, provides structural support. The open-channel topology of $NaSi_4$ is immediately evident: parallel tunnels run through the structure, with accessible diameter sufficient for Na^+ insertion and migration. Such architectural features are known to facilitate fast ion transport and are highly desirable for battery electrodes.

When all Na is removed from $NaSi_4$ (simulating a charged/discharged anode), the silicon host remains intact, yielding a robust porous Si framework with the composition of Si_{16}. As shown in Fig. 1(b), this Si_{16} framework preserves the original channels of $NaSi_4$, demonstrating excellent structural integrity upon desodiation. The ability to maintain an open framework without the guest atoms is a key advantage for cycling stability, as it implies the material can accommodate Na insertion/extraction with minimal structural collapse. The Si_{16} framework has a low density of 1.88 g·cm^{-3} compared to crystalline silicon, reflecting its high porosity. The refined lattice parameters of Si_{16} are a = 3.940 Å, b = 9.946 Å, c = 9.868 Å, and all Si atoms occupy two equivalent Wyckoff 4f sites (0.5000, 0.6146, 0.4724) and (0.7008, 0.2992, 0.8693), consistent with space group *Cmcm*. These details confirm the ordered nature of the porosity: The channels are aligned along the crystallographic a-axis, and are periodically arranged in the b–c

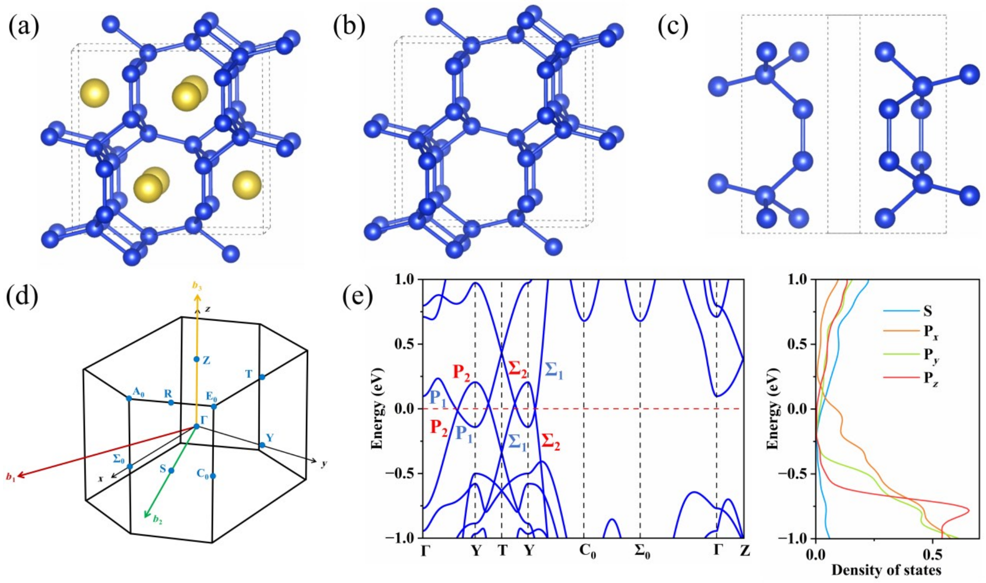

Figure 1 (a) Crystal structure of $NaSi_4$ obtained from structure search, blue and yellow balls symbolize silicon and sodium atoms. (b) Porous Si_{16} framework derived by removing Na from $NaSi_4$. (c) Primitive cell of Si_8. (d) BZ corresponds to the primitive cell. (e) Bulk band structure and band representations of Si_8 along high-symmetry lines, with corresponding DOS and orbital-resolved DOS projections.

plane, providing an array of adsorption sites and diffusion pathways for Na$^+$. We note that this framework can be regarded as an interpenetrating silicene network (ISN) in a sense—it consists of corrugated two-dimensional (2D) silicon sheets that are bonded together into a 3D network, analogous to the previously proposed ISN [43] structure but with a different topology (sp^3 bonds rather than sp^2). The retention of the tunnel structure after Na removal suggests strong Si–Si bonding that does not rely on Na$^+$ for support, which is favorable for long-term cycling.

To evaluate the structural robustness of the pristine Si framework and the sodiated NaSi$_4$ phase, we systematically examined their mechanical, dynamical, and thermal stability. The calculated elastic stiffness tensors (C_{ij}) of pristine Si and NaSi$_4$ (Tables S1 and S2 in the Electronic Supplementary Material (ESM)) exhibit exclusively positive eigenvalues, satisfying the Born mechanical stability criteria and confirming their mechanical stability. The distribution of elastic constants further suggests a moderate elastic anisotropy consistent with their low-symmetry crystal structures. In addition, the phonon dispersions of both systems show no imaginary modes across the entire Brillouin zone (Fig. S1 in the ESM), indicating dynamical stability. *Ab initio* molecular dynamics simulations performed at 500 K reveal only small energy fluctuations without any structural degradation, demonstrating that both structures remain thermally stable well above room temperature.

To facilitate analysis of electronic properties, we reduced the Si$_{16}$ conventional cell to a primitive cell containing 8 Si atoms (denoted Si$_8$, Fig. 1(c)). The corresponding BZ of the primitive cell is shown in Fig. 1(d) with relevant high-symmetry points and paths. All Si atoms in Si$_8$ are equivalent by symmetry, each with four nearest neighbors in a tetrahedral-like arrangement, confirming the sp^3 connectivity. This distinguishes the Si$_{16}$/Si$_8$ framework from other silicon allotropes: Unlike clathrates or channel-containing Zintl phases, where guest atoms stabilize the framework, here the silicon network is inherently stable and strongly bonded.

3.2 Topological semimetallic band structure

The electronic band structure of the silicon framework (Si$_8$) was calculated to investigate its metallicity and any topologically nontrivial features. Figure 1(e) shows the bulk band structure of Si$_8$ along representative high-symmetry directions in the Brillouin zone. The DOS projected onto Si atomic orbitals is plotted alongside. We find that the Si$_8$ framework is intrinsically metallic, with multiple bands crossing the Fermi level. Notably, band crossings occur along the high-symmetry paths Γ–Y–T and Γ–Y–C$_0$ within k_y–k_z and k_x–k_y planes, respectively (here, k_x, k_y, and k_z denote the components of the crystal momentum vector in reciprocal space). These crossing points coincide with mirror planes of the crystal structure. Along the Γ–Y–C$_0$ path, the crossing bands correspond to distinct band representations Σ_1 and Σ_2 and P_1 and P_2, which belong to the point group C_{2v} and mirror symmetry σ.

To confirm the presence of nodal lines, we computed the band dispersion in entire mirror planes. Figures 2(a) and 2(b) map the

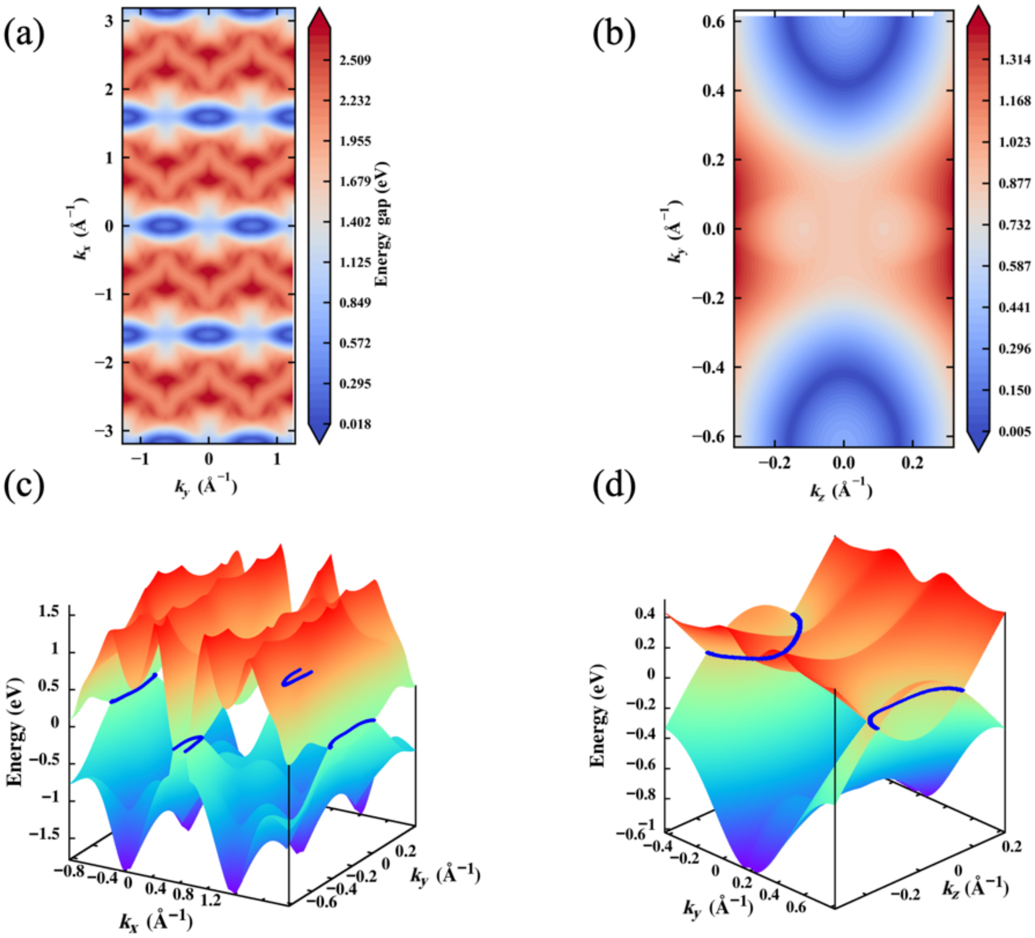

Figure 2 ((a) and (b)) Energy gap between the highest valence band and lowest conduction band in the (a) k_x–k_y and (b) k_y–k_z planes. ((c) and (d)) Band dispersion relationships between VB and CB along corresponding high-symmetry directions in the (c) k_x–k_y and (d) k_y–k_z planes.

energy difference between the conduction band (CB) minimum and valence band (VB) maximum over two orthogonal mirror-invariant planes (corresponding to containing the Y point in the BZ). There are closed loops in these planes where the valence and conduction bands touch, indicating two mirror-symmetry-protected nodal lines encircling the Y point in the BZ. Figures 2(c) and 2(d) further show the band dispersions along cuts through these loops, revealing linear band-crossings at E_F. These results establish that the Si_{16} framework is a TNSM. The nodal lines are centered around the Y point and lie within the mirror planes of the crystal. The approximate energy of the nodal lines lies at or very close to the Fermi level, which is ideal for harnessing the associated high density of states (DOS) for electronic conductivity. The nontrivial topology is further confirmed by the Wilson loop (Wannier charge center) evolution, which exhibits an odd winding behavior on the mirror-invariant planes (see Fig. S2 in the ESM).

A hallmark of topological semimetals is the existence of topologically protected surface states. For nodal-line semimetals, drumhead-like surface bands can appear, connecting the projection of the bulk nodal line on certain surface orientations. To verify this, we calculated the electronic structure of slabs of the Si_{16} framework with different surface terminations. Figure 3 shows the surface band structures for three representative surfaces: (111), $(1\bar{1}1)$, and (001). In all cases, we observe surface-localized bands that span the bulk bandgap region, consistent with the presence of bulk nodal loops. These surface states provide further evidence that the Si_{16} framework is topologically nontrivial. From a practical perspective, the intrinsic electronic conductivity arising from these topological bands is a major advantage for battery electrodes: It means the anode can conduct electrons efficiently without requiring conductive additives or forming an insulating Na compound upon sodiation.

3.3 Na$^+$ adsorption and intercalation thermodynamics

Having established the structural and electronic foundation, we turn to the Na-ion storage properties of the Si_{16} framework. We first examine the energetics of a single Na adsorption in the pristine Si_{16} host by calculating the binding energy (E_b), defined as

$$E_b = E_{NaSi_4} - E_{Si} - \mu_{Na} \tag{2}$$

where E_{NaSi_4} and E_{Si} are the total energies of the Si_{16} host with and without an adsorbed Na atom, respectively, and μ_{Na} is the chemical potential of bulk metallic sodium. The binding energy of a Na atom in the most favorable site is calculated to be E_b = −0.56 eV, where the negative sign indicates exothermic adsorption. This reasonably strong binding suggests that isolated Na$^+$ ions prefer to reside in the silicon framework rather than aggregating as metal, a desirable trait for a battery anode. The magnitude of E_b also indicates a moderate interaction: strong enough to stabilize Na in the host and thereby prevent Na plating, yet not so strong as to make insertion irreversible. For comparison, Na binding on a carbon surface or in graphite is much weaker (positive or near-zero in graphite), whereas in alloy-forming materials like Na–Si phases, it can be much stronger but accompanied by structural change. Thus, the Si_{16} host provides an intermediate binding favorable for intercalation chemistry.

We performed Bader charge analysis to understand the charge transfer upon Na insertion [44]. Each adsorbed Na atom donates approximately 0.81|e| to the silicon host, essentially becoming Na$^+$. The silicon framework, in turn, accumulates this electron density along its lattice (primarily on the Si atoms adjacent to Na). This indicates an ionic bonding character for Na in the Si_{16} channels: The Na loses an electron, and the framework is reduced. Such behavior is consistent with the usual intercalation mechanism in which the anode host acts as a redox center (here, the Si network accepts electrons). We visualized the charge density difference upon Na adsorption in Fig. 4, which clearly shows electron depletion around the Na site and accumulation in the surrounding Si–Si bonds. The significant charge transfer and resultant polarization imply strong electrostatic interactions anchoring Na$^+$ in the channel.

To evaluate how densely Na can be intercalated, we utilized the CE approach. The convex-hull analysis (formation energy vs. composition) for Na_xSi_4 ($0 \le x \le 1$) identified several stable intermediate phases: specifically at compositions x = 0.167, 0.25, 0.50, and 0.667 (Fig. 5(a)). The atomic structures of these intermediates are provided in Fig. S3 in the ESM. Crucially, the fully sodiated $NaSi_4$ (x = 1 and 4 Na per Si_{16}) is also a stable phase. The formation energies are all negative, and no phase separation into Na metal was observed up to x = 1, confirming that the material can reversibly accommodate Na up to the stoichiometric $NaSi_4$ composition. The electronic properties of $NaSi_4$ were further examined by calculating its band structure and density of states. As

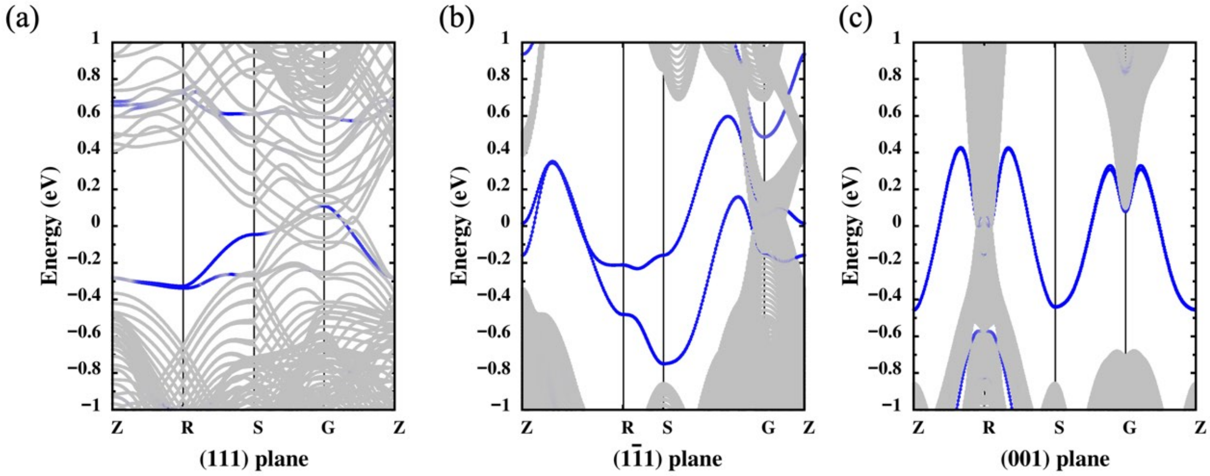

Figure 3 ((a)–(c)) Slab band structures for three surface terminations: (a) (111), (b) $(1\bar{1}1)$, and (c) (001) planes. Gray shading represents projected bulk bands, while blue and red lines indicate surface states.

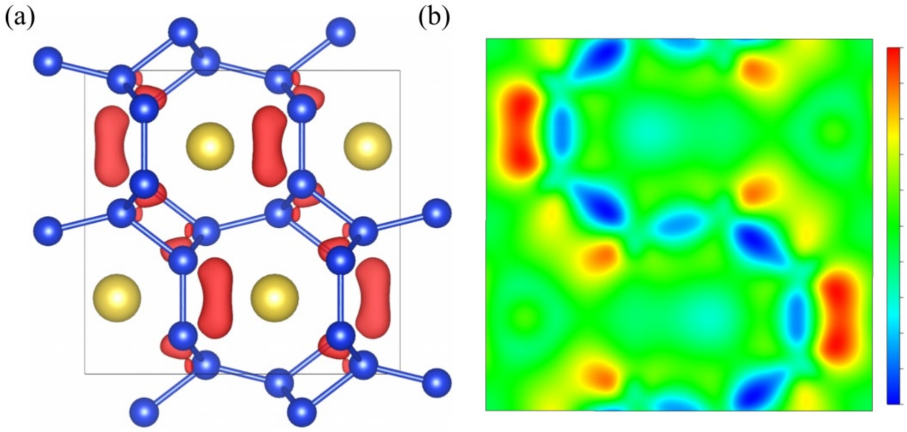

Figure 4 (a) Charge density difference isosurface (isovalue: 0.01 e·Å^{-3}), showing electron accumulation only. (b) Corresponding planar slice on the ab plane. Red denotes electron accumulation; blue indicates depletion.

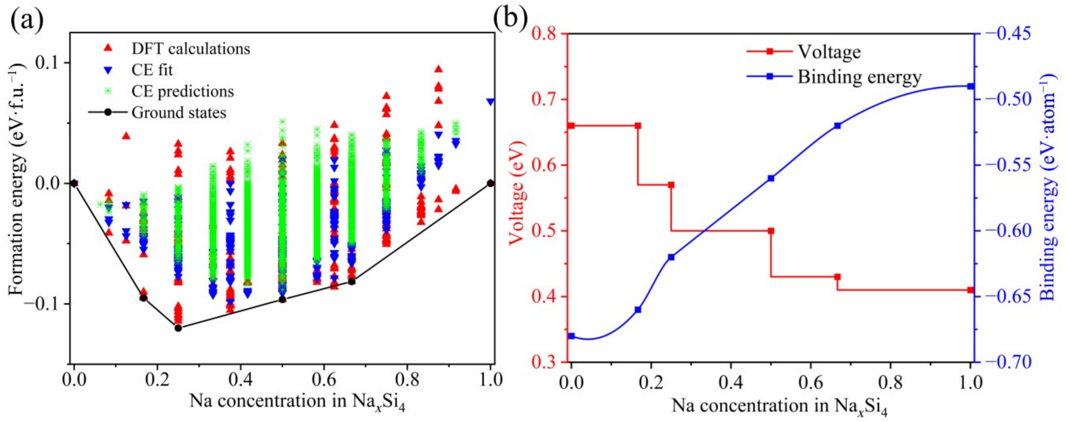

Figure 5 (a) Formation energies of Na$_x$Si$_4$ predicted by the cluster expansion method, highlighting four stable intermediate compositions. (b) The corresponding voltage profile as a function of sodium concentration.

shown in Fig. S4 in the ESM, NaSi$_4$ exhibits a metallic character with finite electronic states at the Fermi level. The projected density of states indicates that the states near the Fermi energy are predominantly contributed by the Si framework, while the contribution from Na is negligible, suggesting that Na mainly acts as a structural template and electron donor rather than participating in electronic transport.

From the set of stable compositions, we constructed the open-circuit voltage (OCV) profile for Na insertion. The computed voltage curves (Fig. 5(b)) show a gently sloping profile with three small plateaus corresponding to two-phase regions between the identified stable phases. Throughout the sodiation from Si$_{16}$ to NaSi$_4$, the voltage remains positive (above 0 V vs. Na/Na$^+$), indicating that sodium insertion is thermodynamically favorable at each step. The average voltage is calculated to be around 0.52 V, with the voltage gradually decreasing from ~ 0.66 V at the early stages (low Na content) to ~ 0.42 V near full Na content. This intermediate voltage (~ 0.5 V) is considered optimal for an anode: It is low enough to yield a high overall cell voltage when paired with typical cathodes, yet high enough to avoid issues like Na metal plating or excessive solid–electrolyte interphase (SEI) formation that occur at very low potentials. In comparison, Si$_{24}$ has an average Na insertion voltage of ~ 0.34 V [29] (quite low, which may increase the risk of Na plating at full charge), whereas ISN's average is ~ 1.35 V [43] (which, while ensuring safe cycling, reduces the energy density significantly). The NaSi$_4$ framework's ~ 0.5 V sits in a favorable middle ground, akin to the carbon TSM anode tC$_{24}$ (0.54 V) [28], balancing energy output and safety.

Using the fully sodiated phase NaSi$_4$, we can deduce the theoretical specific capacity of the anode. In NaSi$_4$, there is one Na atom per formula unit. Considering the mass of just the silicon host (since in practical cells the anode initial weight excludes sodium), the reversible insertion of 1 Na per Si$_4$ corresponds to about 239 mAh·g^{-1} of silicon. This value exceeds the capacities of previously reported crystalline Si frameworks. For instance, Si$_{24}$ can host Na$_4$Si$_{24}$ (4 Na per 24 Si), which is 1 Na per 6 Si ~ 159 mAh·g^{-1}, and ISN hosts NaSi$_6$ (1 Na per 6 Si, 159.5 mAh·g^{-1}). Layered silicene (if it could be used as an anode) can theoretically achieve higher capacities (comparable to graphite's Li capacity, ~ 954 mAh·g^{-1} for Na$_2$Si, though that figure assumes every Si in a freestanding monolayer binds multiple Na) [45], but maintaining a stable structure and electrical connectivity at such high Na content is problematic (and silicene would likely crumple or aggregate). In contrast, the NaSi$_4$ framework allows a large Na uptake in a robust architecture. The calculated capacity of 239 mAh·g^{-1} is also competitive with many state-of-the-art Na-ion anodes; for example, hard carbon achieves 200–300 mAh·g^{-1} [46], Sn$_4$P$_3$ ~ 718 mAh·g^{-1} (but with huge volume change) [47], and conversion oxides typically 300–400 mAh·g^{-1} but often at higher voltage [48]. Thus, NaSi$_4$ offers a moderate capacity while retaining the benefits of an intercalation-type (as opposed to alloy-type) anode.

Importantly, inserting Na into the Si$_{16}$ framework induces only minimal structural strain. Across the full range from $x = 0$ to $x = 1$, our optimized structures show a total volume expansion of < 3%. The lattice expands slightly and uniformly to accommodate Na, without collapsing the channels. A ~ 3% volume change is extraordinarily small compared to conventional Na–Si alloys (which can expand hundreds of percent) [49]. It is even comparable to so-called "zero-strain" materials like $Li_4Ti_5O_{12}$ (which has ~ 0.2% volume change for Li) [50]. Such a small volume change suggests excellent mechanical stability and implies that electrode pulverization or loss of contact would be negligible in this material. The elastic properties in the ESM (Tables S1 and S2 in the ESM) also confirm that $NaSi_4$ maintains mechanical integrity upon sodiation: All elastic constants remain positive and only modestly change with Na content, indicating the framework's stiffness and strength are largely retained. In practice, this means a $NaSi_4$ anode could sustain repeated Na^+ insertion/extraction with long cycle life, as the expansion and contraction of the structure is very small and reversible.

3.4 Na^+ diffusion kinetics

For high power and fast-charge capability, a low energy barrier for Na^+ migration within the anode is essential. Na^+ diffusion channels have an effective diameter of approximately 4 Å (as measured by the framework-to-framework distance along the channel). This size is sufficient to accommodate Na^+ transport but is smaller than the typical molecular dimensions of common carbonate- and ether-based electrolyte solvents, which generally exceed 5–7 Å [51]. As a result, the internal channels are expected to be selectively accessible to Na^+ ions while excluding solvent molecules, thereby limiting electrolyte penetration into the bulk framework. This characteristic is advantageous for suppressing excessive internal SEI formation and improving the initial Coulombic efficiency. We identified likely Na^+ diffusion paths in the Si_{16} framework and calculated their activation energies using CI-NEB (see Fig. 6). There are two distinct channels for Na^+ motion between adjacent sites in this structure: (i) along the main tunnel axis (Path P_1), and (ii) via a narrower crossing between tunnels (Path P_2). Path P_1 runs along the intrinsic one-dimensional channel that goes through the length of the Si_{16} cell, essentially along the *a*-axis. As expected, this is the straightforward route for a Na^+ to hop to a neighboring vacant site in the same channel. Path P_2, in contrast, would require a Na^+ to migrate sideways from one channel to a neighboring channel through a constriction in the framework. This involves passing between silicon ring structures that separate adjacent tunnels. The CI-NEB results (Figs. 6(b) and 6(c)) show a striking difference between these two paths: P_1 exhibits a low diffusion barrier of ~ 0.33 eV, whereas P_2 has a much higher barrier of ~ 2.61 eV. The low barrier for P_1 suggests that Na^+ can readily diffuse along the length of a channel at room temperature, since 0.33 eV is comparable to typical diffusion barriers in intercalation anodes, for instance, Na^+ in TiO_2 (0.3–0.4 eV) [52], in layered MoS_2 (~ 0.28 eV) [53] and is significantly lower than the barrier in Si_{24} (0.80 eV) [54]. On the other hand, the 2.61 eV barrier for P_2 essentially means that cross-channel diffusion is kinetically blocked under normal conditions, Na^+ will not hop between adjacent channels directly through the framework. Fortunately, this does not impede performance because the $NaSi_4$ structure provides continuous pathways along each channel. In a crystal or well-connected particle of the material, Na^+ ions can diffuse rapidly down the tunnels (1D diffusion), and neighboring tunnels are equivalent and all oriented parallel; thus, every Na^+ can find a path to the particle surface by moving along a channel. Although one-dimensional diffusion can be sensitive to local defects, the diffusion channels in this structure are periodically distributed throughout the framework, reducing the likelihood of complete transport blockage in polycrystalline electrodes. In our case, because the channels are regularly arranged, Na^+ can also enter/exit the structure from the ends of channels that intersect the particle surface.

4 Conclusions

In conclusion, we have demonstrated that a porous Na–Si framework ($NaSi_4$) unifies two traditionally separate domains—topological semimetal physics and electrochemical energy storage—within a single silicon-based anode material. Through Na-templated crystal structure prediction and first-principles calculations, we identified an orthorhombic $NaSi_4$ phase composed of interpenetrating sp^3-bonded silicon networks forming one-dimensional channels. Upon Na removal, the resulting Si_{16} host preserves the open-channel framework and is intrinsically a topological nodal-line semimetal, characterized by symmetry-protected band crossings and robust electronic conductivity. This topology-derived intrinsic conductivity directly overcomes the long-standing limitation of poor electronic transport in silicon anodes. At the same time, the open-channel architecture enables efficient sodium storage, delivering a reversible capacity of 239 $mAh \cdot g^{-1}$ at a moderate operating voltage (~ 0.5 V vs. Na/Na^+), fast one-dimensional Na^+ diffusion with a low migration barrier (~ 0.33 eV), and exceptional dimensional stability with less than 3% volume

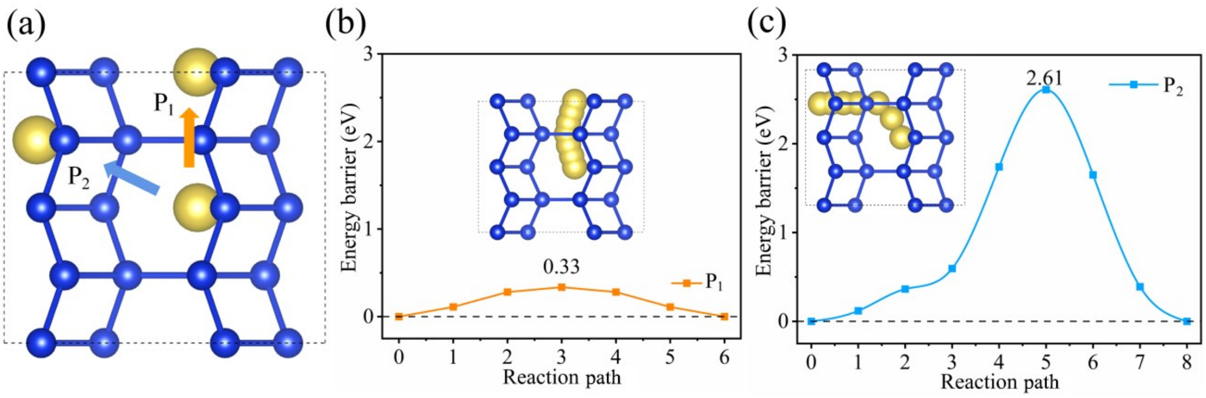

Figure 6 (a) Na^+ migration paths (P_1 and P_2) between adjacent adsorption sites. ((b) and (c)) Corresponding diffusion energy profiles.

expansion upon full sodiation. Compared with previously reported silicon allotropes and carbon-based anodes, $NaSi_4$ achieves a rare combination of moderate capacity, favorable kinetics, and low-strain reversibility within a rigid all-silicon framework.

Beyond the specific Na–Si system, this work establishes a general design paradigm in which electronic topology and ion-storage functionality are intrinsically coupled. By exploiting symmetry-protected metallic states and topology-constrained geometries, battery electrodes can be designed to simultaneously achieve high conductivity, structural resiliency, and efficient ion transport. This study represents the first example of an all-silicon nodal-line semimetal proposed as a sodium-ion battery anode and highlights an unexplored pathway toward multifunctional energy materials. We anticipate that these findings will stimulate further experimental and theoretical efforts at the intersection of topological quantum materials and electrochemical storage, opening new opportunities for next-generation, high-performance battery systems.

Electronic Supplementary Material: Supplementary material (additional details supporting the main text, including the calculated elastic constants of pristine Si and $NaSi_4$ (Tables S1 and S2), phonon dispersions and *ab initio* molecular dynamics results confirming the structural stability (Fig. S1), Wilson loop spectra demonstrating the nontrivial band topology (Fig. S2), atomic configurations of the four stable intermediate Na_xSi_4 phases identified from cluster expansion analysis (Fig. S3), and the electronic band structure together with total and projected DOS of $NaSi_4$ (Fig. S4)) is available in the online version of this article at https://doi.org/10.26599/NR.2026.94908585.

Data availability

All data needed to support the conclusions in the paper are presented in the manuscript and the Electronic Supplementary Material. Additional data related to this paper may be requested from the corresponding author upon request.

Acknowledgements

This work was supported by the Natural Science Foundation of Shanxi Province (No. 202203021212410) and the Key Laboratory of Magnetic Molecules and Magnetic Information Materials of the Ministry of Education (No. 010520240018). We gratefully acknowledge Hongzhiwei Technology (HZWTECH) for providing computational resources. H. H. X. acknowledges the support from China Scholarship Council (No. 202308140072).

Declaration of competing interest

All the contributing authors report no conflict of interests in this work.

Author contribution statement

H. H. X.: Conceptualization, methodology, investigation, formal analysis, validation, writing – original draft, project administration. Y. N. S.: Data curation, investigation, formal analysis. K. H. Z.: Data curation, validation. J. K. S.: Data curation, formal analysis. Y. H. L.: Supervision, writing – review & editing. All the authors have approved the final manuscript.

Use of AI statement

During the preparation of this manuscript, the authors used ChatGPT (developed by OpenAI) for language editing and improvement. The authors reviewed and verified all content for accuracy and take full responsibility for the final manuscript.

References

[1] Tian, Y. S.; Zeng, G. B.; Rutt, A.; Shi, T.; Kim, H.; Wang, J. Y.; Koettgen, J.; Sun, Y. Z.; Ouyang, B.; Chen, T. N. et al. Promises and challenges of next-generation “beyond Li-ion” batteries for electric vehicles and grid decarbonization. *Chem. Rev.* **2021**, *121*, 1623–1669.

[2] Zhang, X.; Yang, Y. A.; Zhou, Z. Towards practical lithium-metal anodes. *Chem. Soc. Rev.* **2020**, *49*, 3040–3071.

[3] Wu, F. X.; Maier, J.; Yu, Y. Guidelines and trends for next-generation rechargeable lithium and lithium-ion batteries. *Chem. Soc. Rev.* **2020**, *49*, 1569–1614.

[4] Tse, Y. T.; Lu, S. B.; Sun, X. Y.; Zhang, D. C.; Hui, K. C.; Liu, C. M.; Zhi, C. Y. High dielectric composite polymer electrolyte for lithium-ion batteries. *Nano Res.* **2025**, *18*, 94907260.

[5] Usiskin, R.; Lu, Y. X.; Popovic, J.; Law, M.; Balaya, P.; Hu, Y. S.; Maier, J. Fundamentals, status and promise of sodium-based batteries. *Nat. Rev. Mater.* **2021**, *6*, 1020–1035.

[6] Chen, M. Z.; Hua, W. B.; Xiao, J.; Zhang, J. L.; Lau, V. W. H.; Park, M.; Lee, G. H.; Lee, S.; Wang, W. L.; Peng, J. et al. Activating a multielectron reaction of NASICON-structured cathodes toward high energy density for sodium-ion batteries. *J. Am. Chem. Soc.* **2021**, *143*, 18091–18102.

[7] Habib, L.; Suo, G. Q.; Li, J. R.; Lin, C. J.; Luo, X. C.; Yang, G. L.; Kalkozova, Z. K.; Naseem, K. Interface and structural modulation stabilization strategies for layered transition metal oxide cathodes in sodium-ion batteries. *Energy Storage Mater.* **2026**, *84*, 104863.

[8] Perveen, T.; Siddiq, M.; Shahzad, N.; Ihsan, R.; Ahmad, A.; Shahzad, M. I. Prospects in anode materials for sodium ion batteries—A review. *Renew. Sustain. Energy Rev.* **2020**, *119*, 109549.

[9] Luo, Z. H.; Zhang, D.; Guo, J. X.; Jiang, F.; Shen, N. L.; Du, Y. F.; Jiang, Z. J.; Wang, T.; Liu, X.; Cheng, X. B. et al. Recent progress on the materials design towards thermally safe sodium-ion batteries. *J. Energy Chem.* **2025**, *102*, 555–575.

[10] He, H. N.; Li, X. L.; Huang, D.; Luan, J. Y.; Liu, S. L.; Pang, W. K.; Sun, D.; Tang, Y. E.; Zhou, W. Z.; He, L. R. et al. Electron-injection-engineering induced phase transition toward stabilized 1T-MoS_2 with extraordinary sodium storage performance. *ACS Nano* **2021**, *15*, 8896–8906.

[11] Wu, C.; Dou, S. X.; Yu, Y. The state and challenges of anode materials based on conversion reactions for sodium storage. *Small* **2018**, *14*, 1703671.

[12] Liu, K.; Ji, S. P.; Liu, B. Y.; Zeng, X. Y.; Zhang, Y. J.; Wu, X. Q.; Zhou, X. Z.; Xiao, J.; Li, L.; Zhang, Y. J. Recent advances on coal-based hard carbon anode materials for sodium-ion batteries. *Nano Res.* **2025**, *18*, 94907625.

[13] Dong, Y. Q.; Ning, Y. B.; Zhou, L.; Dong, S. W.; Qiang, Z. M.; Lin, K.; Li, D. L.; Guan, L.; Lou, S. F. Pre-sodiation strategies for high reversibility of hard carbon anodes: A review. *J. Energy Chem.* **2026**, *115*, 892–903.

[14] Li, J. R.; Suo, G. Q.; Lin, C. J.; Li, J. Z.; Luo, X. C.; Yang, G. L.; Habib, L.; Kalkozova, Z. K.; Naseem, K. Synergistic electron highways and mechanical buffering in a dual-carbon confined MoS_2 anode for superior sodium-ion storage. *Chem. Eng. J.* **2026**, *529*, 173031.

[15] Li, Y.; Wu, F.; Li, Y.; Feng, X.; Zheng, L. M.; Liu, M. Q.; Li, S. Q.; Qian, J.; Wang, Z. H.; Ren, H. X. et al. Multilevel gradient-ordered silicon anode with unprecedented sodium storage. *Adv. Mater.* **2024**, *36*, 2310270.

[16] Tsai, P. C.; Chung, S. C.; Lin, S. K.; Yamada, A. *Ab initio* study of sodium intercalation into disordered carbon. *J. Mater. Chem. A* **2015**, *3*, 9763–9768.

[17] Wang, E. H.; Chen, M. Z.; Guo, X. D.; Chou, S. L.; Zhong, B. H.; Dou, S. X. Synthesis strategies and structural design of porous carbon-incorporated anodes for sodium-ion batteries. *Small Methods* **2020**, *4*, 1900163.

[18] Wang, Y. X.; Li, M.; Zhang, Y.; Zhang, N. Q. Hard carbon for sodium storage: Mechanism and performance optimization. *Nano Res.* **2024**, *17*, 6038–6057.

[19] Chevrier, V. L.; Ceder, G. Challenges for Na-ion negative electrodes. *J. Electrochem. Soc.* **2011**, *158*, A1011.

[20] Habib, L.; Suo, G. Q.; Habib, N.; Aqdas, M.; Lin, C. J.; Li, J. R.; Javed, S. MoS$_2$-based anodes for sodium-ion batteries: Recent developments and key engineering approaches. *J. Energy Storage* **2025**, *139*, 118821.

[21] Jin, X.; Wang, X. F.; Liu, Y. L.; Kim, M.; Cao, M.; Xie, H. H.; Liu, S. T.; Wang, X. B.; Huang, W.; Nanjundan, A. K. et al. Nitrogen and sulfur co-doped hierarchically porous carbon nanotubes for fast potassium ion storage. *Small* **2022**, *18*, 2203545.

[22] Muhammad, I.; Younis, U.; Xie, H. H.; Khan, A. A.; Khaliq, A.; Samad, A.; Schwingenschlögl, U.; Sun, Q. Borophene-based three-dimensional porous structures as anode materials for alkali metal-ion batteries with ultrahigh capacity. *Chem. Mater.* **2021**, *33*, 2976–2983.

[23] Liu, J. Y.; Wang, S.; Sun, Q. All-carbon-based porous topological semimetal for Li-ion battery anode material. *Proc. Natl. Acad. Sci. USA* **2017**, *114*, 651–656.

[24] Liu, J. Y.; Wang, S.; Qie, Y.; Yu, J. B.; Sun, Q. A new porous metallic silicon dicarbide for highly efficient Li-ion battery anode identified by targeted structure search. *Carbon* **2018**, *140*, 680–687.

[25] Luo, H. X.; Yu, P. F.; Li, G. W.; Yan, K. Topological quantum materials for energy conversion and storage. *Nat. Rev. Phys.* **2022**, *4*, 611–624.

[26] Xie, H. H.; Qie, Y.; Imran, M.; Sun, Q. Topological semimetal porous carbon as a high-performance anode for Li-ion batteries. *J. Mater. Chem. A* **2019**, *7*, 14253–14259.

[27] Xie, H. H.; Qie, Y.; Muhammad, I.; Sun, Q. B$_4$ cluster-based 3D porous topological metal as an anode material for both Li- and Na-ion batteries with a superhigh capacity. *J. Phys. Chem. Lett.* **2021**, *12*, 1548–1553.

[28] Qie, Y.; Liu, J. Y.; Wang, S.; Sun, Q.; Jena, P. Tetragonal C$_{24}$: A topological nodal-surface semimetal with potential as an anode material for sodium ion batteries. *J. Mater. Chem. A* **2019**, *7*, 5733–5739.

[29] Kim, D. Y.; Stefanoski, S.; Kurakevych, O. O.; Strobel, T. A. Synthesis of an open-framework allotrope of silicon. *Nat. Mater.* **2015**, *14*, 169–173.

[30] Wang, Y. C.; Lv, J.; Zhu, L.; Ma, Y. M. CALYPSO: A method for crystal structure prediction. *Comput. Phys. Commun.* **2012**, *183*, 2063–2070.

[31] Wang, Y. C.; Lv, J.; Zhu, L.; Ma, Y. M. Crystal structure prediction via particle-swarm optimization. *Phys. Rev. B* **2010**, *82*, 094116.

[32] Kresse, G.; Furthmüller, J. Efficient iterative schemes for *ab initio* total-energy calculations using a plane-wave basis set. *Phys. Rev. B* **1996**, *54*, 11169–11186.

[33] Kresse, G.; Furthmüller, J. Efficiency of *ab initio* total energy calculations for metals and semiconductors using a plane-wave basis set. *Comput. Mater. Sci.* **1996**, *6*, 15–50.

[34] Blöchl, P. E. Projector augmented-wave method. *Phys. Rev. B* **1994**, *50*, 17953–17979.

[35] Perdew, J. P.; Burke, K.; Ernzerhof, M. Generalized gradient approximation made simple. *Phys. Rev. Lett.* **1996**, *77*, 3865–3868.

[36] Monkhorst, H. J.; Pack, J. D. Special points for Brillouin-zone integrations. *Phys. Rev. B* **1976**, *13*, 5188–5192.

[37] *Device Studio*, Version 2021A; Hongzhiwei Technology (Shanghai) Co., Ltd.: Shanghai, China, 2021.

[38] Pizzi, G.; Vitale, V.; Arita, R.; Blügel, S.; Freimuth, F.; Géranton, G.; Gibertini, M.; Gresch, D.; Johnson, C.; Koretsune, T. et al. Wannier90 as a community code: New features and applications. *J. Phys.: Condens. Matter* **2020**, *32*, 165902.

[39] Wu, Q. S.; Zhang, S. N.; Song, H. F.; Troyer, M.; Soluyanov, A. A. WannierTools: An open-source software package for novel topological materials. *Comput. Phys. Commun.* **2018**, *224*, 405–416.

[40] Henkelman, G.; Uberuaga, B. P.; Jónsson, H. A climbing image nudged elastic band method for finding saddle points and minimum energy paths. *J. Chem. Phys.* **2000**, *113*, 9901–9904.

[41] De Fontaine, D. Cluster approach to order–disorder transformations in alloys. *Solid State Phys.* **1994**, *47*, 33–176.

[42] Van De Walle, A.; Ceder, G. Automating first-principles phase diagram calculations. *J. Phase Equilib.* **2002**, *23*, 348–359.

[43] Qie, Y.; Liu, J. Y.; Li, X. Y.; Wang, S.; Sun, Q.; Jena, P. Interpenetrating silicene networks: A topological nodal-line semimetal with potential as an anode material for sodium ion batteries. *Phys. Rev. Mater.* **2018**, *2*, 084201.

[44] Yu, M.; Trinkle, D. R. Accurate and efficient algorithm for Bader charge integration. *J. Chem. Phys.* **2011**, *134*, 064111.

[45] Zhuang, J. C.; Xu, X.; Peleckis, G.; Hao, W. C.; Dou, S. X.; Du, Y. Silicene: A promising anode for lithium-ion batteries. *Adv. Mater.* **2017**, *29*, 1606716.

[46] Slater, M. D.; Kim, D.; Lee, E.; Johnson, C. S. Sodium-ion batteries. *Adv. Funct. Mater.* **2013**, *23*, 947–958.

[47] Qian, J. F.; Xiong, Y.; Cao, Y. L.; Ai, X. P.; Yang, H. X. Synergistic Na-storage reactions in Sn$_4$P$_3$ as a high-capacity, cycle-stable anode of Na-ion batteries. *Nano Lett.* **2014**, *14*, 1865–1869.

[48] Yabuuchi, N.; Kubota, K.; Dahbi, M.; Komaba, S. Research development on sodium-ion batteries. *Chem. Rev.* **2014**, *114*, 11636–11682.

[49] Lao, M. M.; Zhang, Y.; Luo, W. B.; Yan, Q. Y.; Sun, W. P.; Dou, S. X. Alloy-based anode materials toward advanced sodium-ion batteries. *Adv. Mater.* **2017**, *29*, 1700622.

[50] Ohzuku, T.; Ueda, A.; Yamamoto, N. Zero-strain insertion material of Li[Li$_{1/3}$Ti$_{5/3}$]O$_4$ for rechargeable lithium cells. *J. Electrochem. Soc.* **1995**, *142*, 1431.

[51] Xu, K. Electrolytes and interphases in Li-ion batteries and beyond. *Chem. Rev.* **2014**, *114*, 11503–11618.

[52] Vasileiadis, A.; Wagemaker, M. Thermodynamics and kinetics of Na-ion insertion into hollandite-TiO$_2$ and O3-layered NaTiO$_2$: An unexpected link between two promising anode materials for Na-ion batteries. *Chem. Mater.* **2017**, *29*, 1076–1088.

[53] Massaro, A.; Pecoraro, A.; Muñoz-García, A. B.; Pavone, M. First-principles study of Na intercalation and diffusion mechanisms at 2D MoS$_2$/graphene interfaces. *J. Phys. Chem. C* **2021**, *125*, 2276–2286.

[54] He, Y.; Lu, X.; Kim, D. Y. A first-principles study on Si$_{24}$ as an anode material for rechargeable batteries. *RSC Adv.* **2018**, *8*, 20228–20233.